Biochemical, histological and behavioral characterization of a new mouse model of Niemann-Pick C2 disease

Elias G[1,2], Marcó S[1,2,4], Sánchez X[1,2], Ribera A[1,2,4], Sánchez V[1,2], Bertolin J[1,2], Pérez J[1,2], Roca C[1,2,4], García M[1,2,4], Molas M[1,2,4], León X[1,2], Ruberte J[1,3], Storch J[1,2] and Bosch F[1,2,4].

[1]Center of Animal Biotechnology and Gene Therapy, Departments of [2]Biochemistry and Molecular Biology and [3]Animal Health and Anatomy, School of Veterinary Medicine, Universitat Autònoma de Barcelona, Bellaterra, 08193 and [4]Centro de Investigación Biomédica en Red de Diabetes y Enfermedades Metabólicas Asociadas (CIBERDEM), Madrid, Spain.

Background: The Niemann-Pick C2 (NPC2) disease is an ultra-rare autosomal recessive Lysosomal Storage Disease (LSD) caused by deficiency of Niemann-Pick C2 protein. NPC2 is involved in the egress of unesterified cholesterol from the late endosome/lysosome compartment to other parts of the cell. As a consequence, pathologic accumulation of cholesterol in lysosomes occurs, which leads to cellular damage. Clinically, patients exhibit neurodegeneration due to progressive neuronal death, hepatosplenomegaly, lung deficiency and reduced life expectancy. To date, only substrate reduction therapy is approved for the treatment of NPC2, with limited efficacy.
Methods: Npc2$^{-/-}$ mouse model was analyzed at 15, 30, 45 and 60 days of age to detect the age of onset and the course of the NPC2 disease.
Results: Here, we report the characterization of a new NPC2 mouse model generated by targeted disruption of the Npc2 gene. Starting at 1 month of age, NPC2-deficient mice showed signs of CNS pathology which included accumulation of unesterified cholesterol, lysosomal distension and dysfunction, hypomyelinitation, neuroinflammation and reduced brain weight. Evidence of impaired autophagy was detected in the cerebellum, which lead to a drastic reduction in Purkinje cell density at 2 months of age. In the periphery, cholesterol accumulation was observed in most organs analysed, but lysosomal pathology seemed most severe in liver. NPC2-deficient mice also showed progressive hepatosplenomegaly and body weight loss. Finally, NPC2-deficient mice had severely shortened lifespan as well as evident behavioural alterations, ataxic gait and reduced exploratory activity, all of which worsened over time.
Conclusions: Altogether, these results demonstrated that this animal model recapitulated human NPC2 disease, providing a valuable tool to gain insight into the physiopathology of the disease and for the development of novel therapeutic approaches for NPC2 patients.

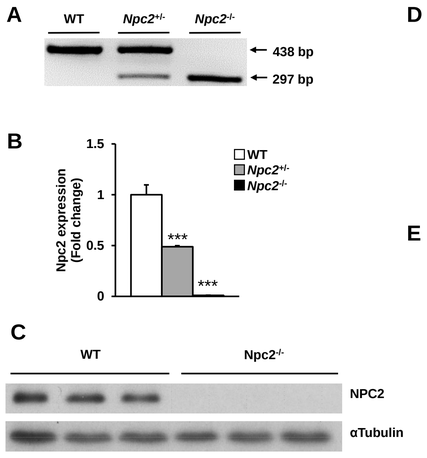

Figure 1. Generation of an NPC2 knockout mice. (A) Representative image of an agarose gel showing the PCR amplicons obtained when genotyping WT (*Npc2*$^{+/+}$), heterozygous (*Npc2*$^{+/-}$) and homozygous (*Npc2*$^{-/-}$) mice. **(B)** *Npc2* expression in liver of 2-month-old WT, heterozygous and *Npc2*$^{-/-}$ male mice. **(C)** Western blot of NPC2 protein in liver of 2-month-old male mice. **(D)** Analysis of body weight of WT and *Npc2*$^{-/-}$ mice. n=11 for WT mice and 7 for *Npc2*$^{-/-}$ mice. **(E)** Kaplan-Meier analysis of survival. n=20 for WT mice and 18 for *Npc2*$^{-/-}$ mice. Values are expressed as mean±SEM. **P*<0.05, ***P*<0.01 and ****P*<0.001.

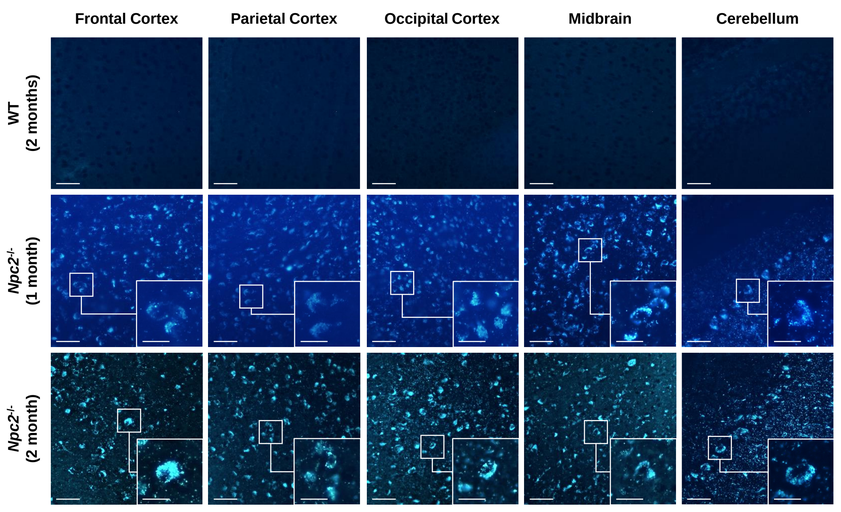

Figure 2. Non-esterified cholesterol accumulation in neuron soma of NPC2-deficient mice. Photomicrographs of the fluorescent staining with Filipin Complex, which binds to non-esterified cholesterol, of brain sections in WT and *Npc2*$^{-/-}$ mice at 1 and 2 months of age. Representative images of 5 animals/group. Scale bar: 50 µm; insets, 20 µm.

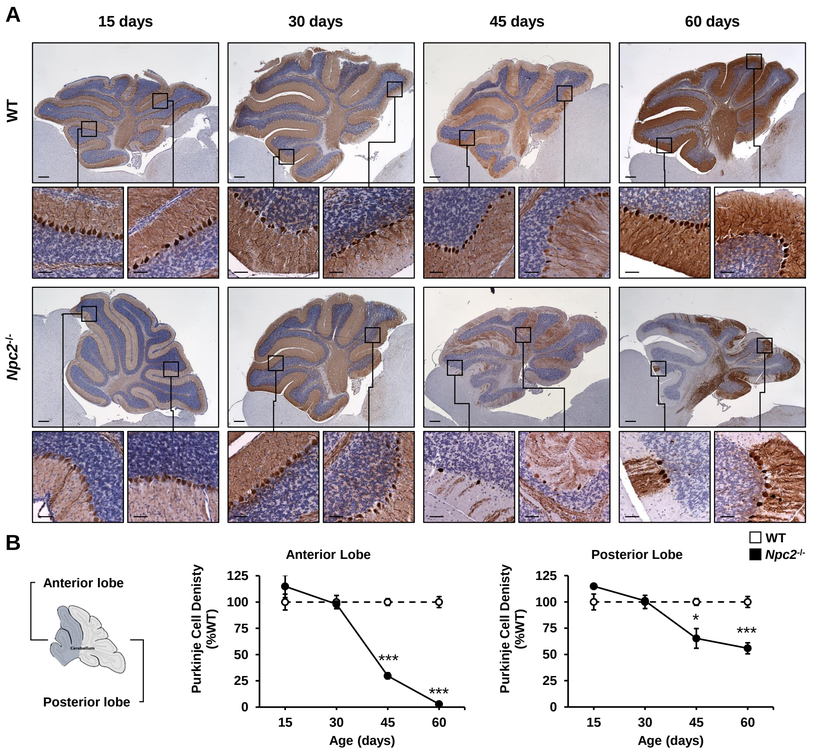

Figure 3. Progressive Purkinje cell loss in NPC2-deficient mice. (A) Representative photomicrographs of the immunostaining for the Purkinje cell marker Calbindin D-28K in cerebellum sections of WT and *Npc2*$^{-/-}$ mice aged 15, 30, 45 and 60 days. Scale bar: 500 µm; insets, 50 µm. **(B)** Purkinje cell density quantification in the anterior lobe and posterior lobe of the same cerebellum sections as in (A). Values are expressed as mean±SEM of 4-5 animals/group. **P*<0.05 and ****P*<0.001.

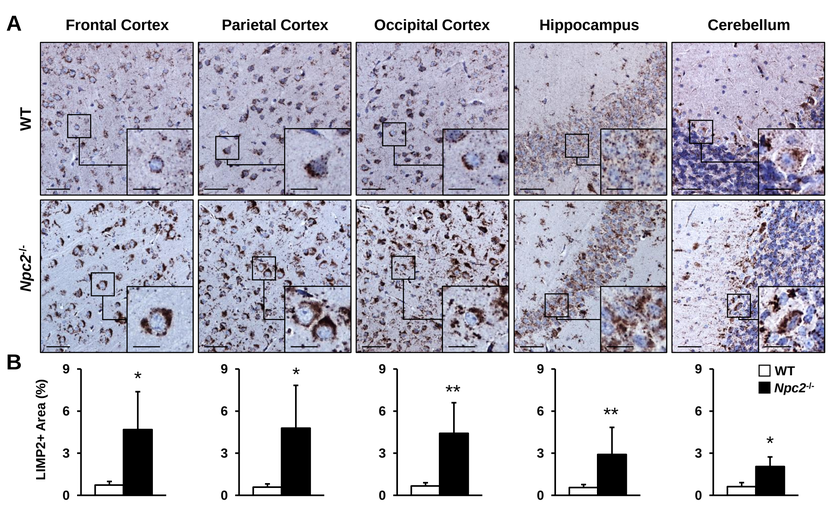

Figure 4. Lysosomal distension in the CNS of NPC2-deficient mice. (A) Representative photomicrographs of the immunostaining for the lysosomal marker LIMP2 in brain sections of WT and *Npc2*$^{-/-}$ male mice at 2 months of age. Scale bar: 50 µm; insets, 20 µm. **(B)** Percentage of LIMP2 positive area in each brain region. Values are expressed as mean±SEM of 5 animals/group. **P*<0.05 and ***P*<0.01.

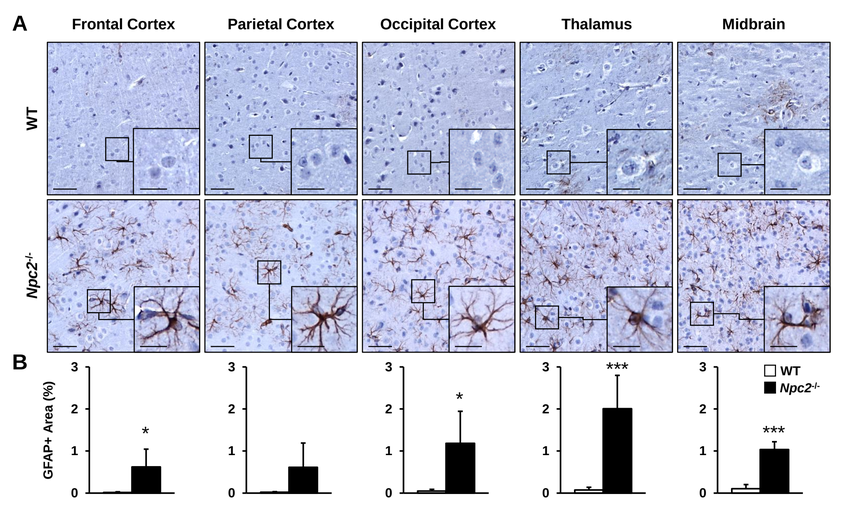

Figure 5. Astrogliosis in the CNS of NPC2-deficient mice. (A) Representative photomicrographs of the immunostaining for the astrocyte marker GFAP in brain sections of WT and *Npc2*$^{-/-}$ male mice at 2 months of age. Scale bar: 50 µm; insets, 20 µm. **(B)** Percentage of GFAP positive area in each brain region. Values are expressed as mean±SEM of 5 animals/group. **P*<0.05 and ****P*<0.001.

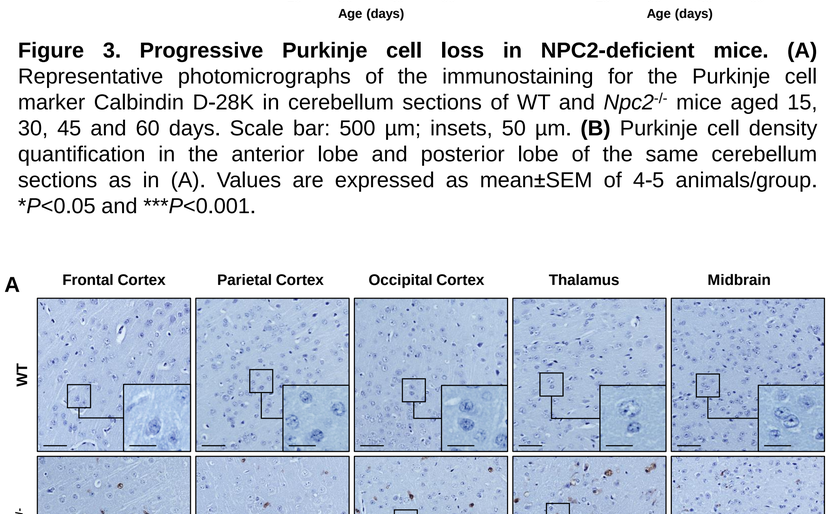

Figure 6. Microgliosis in the CNS of NPC2-deficient mice. (A) Representative photomicrographs of the staining with the lectin BSI-B4, which binds to microglia, in brain sections of WT and *Npc2*$^{-/-}$ male mice at 2 months of age. Scale bar: 50 µm; insets, 20 µm. **(B)** Percentage of BSI-B4 positive area in each brain region. Values are expressed as mean±SEM of 5 animals/group. **P*<0.05, ***P*<0.01 and ****P*<0.001.

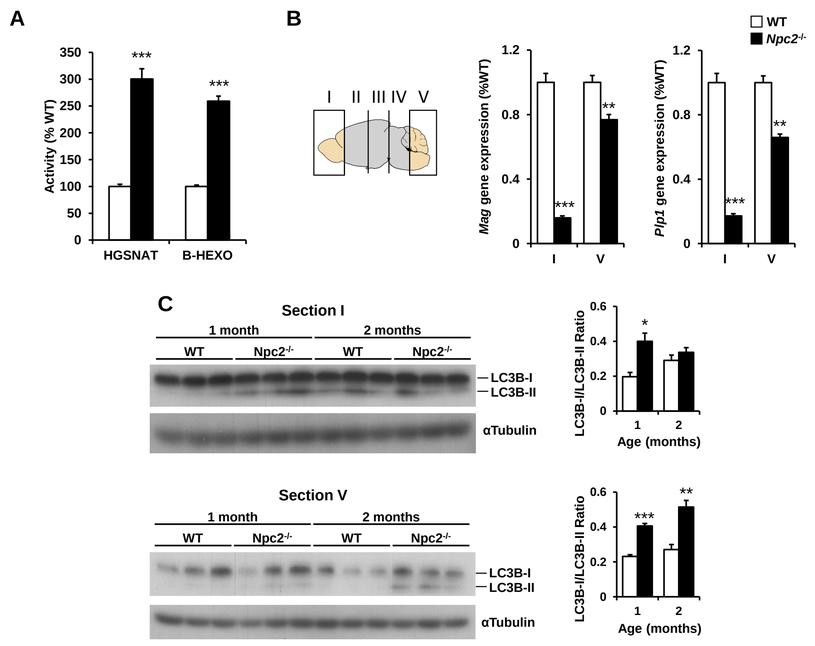

Figure 7. Pathological consequences of cholesterol accumulation in the lysosome. Assessment of the CNS pathology in NPC2-deficient male mice. **(A)** Enzymatic activity of lysosomal enzymes enzymes, expressed as percentage of WT activity, at 2 months of age. **(B)** Gene expression of *Mag* and *Plp1*, involved in myelin biogenesis, in 2 sagittal brain sections of 2-month-old mice. **(C)** Western blot analysis of LC3B, a marker of autophagic flux, in the same brain sections as in *(C)* at 1 and 2 months of age. Values are expressed as mean±SEM of 5 animals/group in (A) and (B) and 3 animals/group in (C). **P*<0.05, ***P*<0.01 and ****P*<0.001.

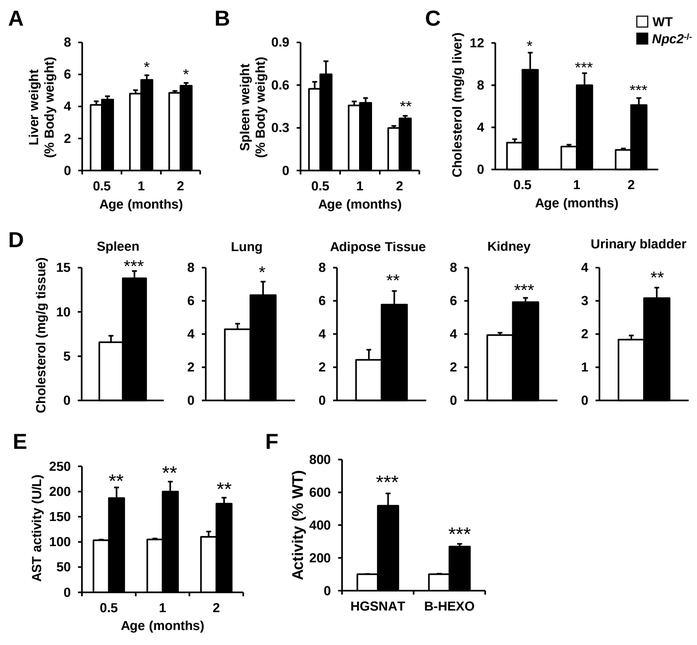

Figure 8. Somatic pathology in NPC2-deficient mice. (A,B) Weight of liver (A) and spleen (B) relative to body weight of male mice at 15 days, 1 and 2 months of age. **(C)** Total cholesterol quantification in liver extracts of WT and NPC2-deficient mice at different ages. **(D)** Total cholesterol quantification in somatic tissue extracts at 2 months of age. **(E)** Assessment of AST activity, in serum at 15 days, 1 and 2 months. **(F)** Enzymatic activity of lysosomal enzymes in liver extracts, expressed as percentage of WT activity, at 2 months of age. Values are expressed as mean±SEM of 4 (15 days) and 15 animals/group (1 and 2 months) in (A), (B) and (C) and 5 animals/group in (D), (E) and (F). **P*<0.05, ***P*<0.01 and ****P*<0.001.

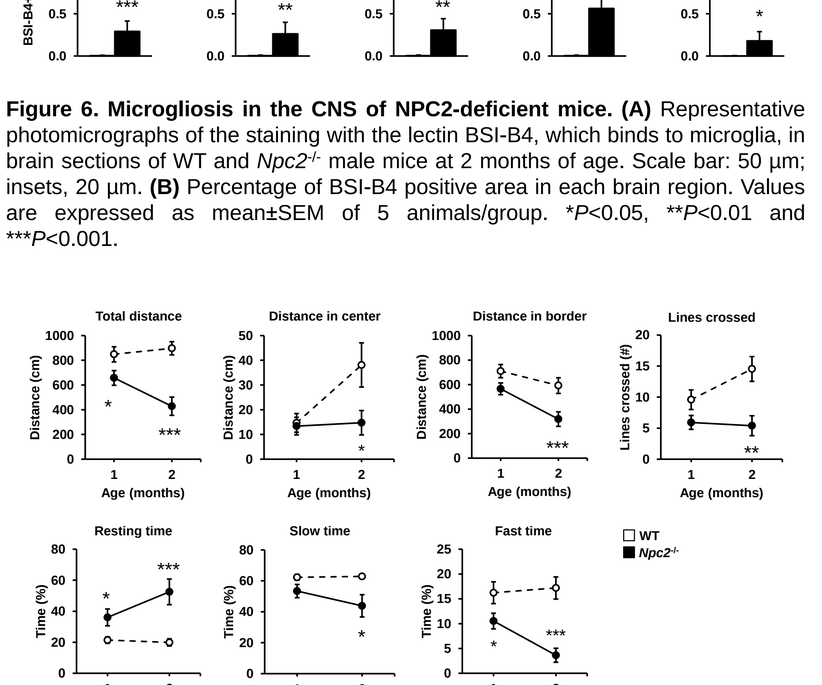

Figure 9. Behavior alteration in NPC2-deficient mice. Evaluation of locomotor and exploratory activity in the Open Field test in naïve WT and NPC2-deficient male mice aged 1 and 2 months. Values are expressed as mean±SEM of 14-15 animals/group. **P*<0.05, ***P*<0.01 and ****P*<0.001.

Mice deficient in NPC2 protein at 2 month of age showed pathological alterations in the CNS, such as generalized unesterified cholesterol accumulation in neuron soma, progressive Purkinje cell death, lysosomal distension, neuroinflammation, hypomyelination and had autophagic flux dysregulation by the age of 2 months. Hepatosplenomegaly was observed and cholesterol accumulated in several somatic tissue analyzed. Finally, NPC2-deficient mice also presented progressive behavioral alterations. Altogether, these results demonstrate that this NPC2 mouse model recapitulates the main hallmarks of the human disease, thus providing a new tool to further study the physiopathology of the disease and for the development of novel gene therapy strategies to treat NPC2 patients.

This research has been supported by grants from Plan Nacional I+D+I from the Ministerio de Ciencia e Innovación and the European Union through Regional Development Funds (FEDER) (PID 2020-113864RB-100, «Proyectos de I+D+i» Retos Investigación 2020)